Fermi velocity renormalization and dynamical gap generation in graphene

C. Popovici,[1] C. S. Fischer,[1] and L. von Smekal[1,2]
[1]*Institut für Theoretische Physik, Justus-Liebig-Universität Giessen, Heinrich-Buff-Ring 16, 35392 Giessen, Germany*
[2]*Theoriezentrum, Institut für Kernphysik, Technische Universität Darmstadt, 64289 Darmstadt, Germany*
(Received 30 August 2013; published 27 November 2013)

We study the renormalization of the Fermi velocity by the long-range Coulomb interactions between the charge carriers in the Dirac-cone approximation for the effective low-energy description of the electronic excitations in graphene at half-filling. Solving the coupled system of Dyson-Schwinger equations for the dressing functions in the corresponding fermion propagator with various approximations for the particle-hole polarization, we observe that Fermi velocity renormalization effects generally lead to a considerable increase of the critical coupling for dynamical gap generation and charge-density-wave formation at the semimetal-insulator transition.

DOI: 10.1103/PhysRevB.88.205429 PACS number(s): 71.10.Hf, 73.22.Pr, 71.27.+a, 11.15.Tk

I. INTRODUCTION

Since its synthesis in 2004,[1,2] graphene has revealed fascinating electronic properties, such as the anomalous quantum Hall effect,[3,4] Klein tunneling,[5,6] or charge confinement[7] (comprehensive overviews can be found in Refs. 8–11). It has been known for a long time from a simple noninteracting tight-binding model[12,13] that graphene's two-dimensional honeycomb lattice is special in that its quasiparticle dispersion relation for low-energy excitations around charge neutrality at two independent Dirac points in the first Brillouin zone is linear, $E_k = \pm v_F|k|$, where $v_F \sim 10^6$ m/s $\approx c/300$ is the Fermi velocity and $k = (k_x, k_y)$ is the momentum of the fermionic quasiparticle in two dimensions. The tight-binding Hamiltonian effectively reduces to a free Dirac Hamiltonian. This quasirelativistic regime for low-energy excitations is separated from the nonrelativistic excitation spectrum at higher energies by a van Hove singularity in the density of states. Thus, already the tight-binding model also serves as a simple example of an excited-state phase transition[14] which in this case reflects the presence of a topological electronic ground-state transition when the chemical potential is tuned away from half-filling and beyond the van Hove singularity, where the static susceptibility diverges logarithmically, indicative of a neck-disrupting Lifshitz transition in two dimensions.

Within field theory descriptions of the electronic excitations in graphene, charge fractionalization and vortex formation have been described through chiral gauge models[15–17] which include the dynamics of the carbon background and doping effects. Charge confinement and Klein tunneling were investigated within such a model in Ref. 18. Cosmological models were used to describe the electronic properties of deformed graphene sheets,[19] topological defects, and curvature as described by geometric gauge fields that also lead to an index theorem for graphene.[20] The various uses of gauge fields to model topological defects as well as stress and strain on graphene sheets are reviewed in Ref. 21. The effects of additional short-range four-fermion couplings to model phonon interactions have been investigated at mean-field level in Ref. 22, and more recently within the functional renormalization group approach in Refs. 23 and 24.

The importance of many-body interactions in graphene has been established both theoretically (see Ref. 9 and references therein, for example) and experimentally (in a recent measurement of the Fermi velocity at low energies,[25] but also from the observation of a gap in an ARPES measurement of epitaxial graphene, upon dosing with small amounts of atomic hydrogen[26]). Long-range electron-electron interactions induce a momentum-dependent renormalization of the Fermi velocity. If the Coulomb interaction can be made sufficiently strong, one furthermore expects that a mass gap is dynamically generated, analogous to chiral symmetry breaking in QCD, such that graphene undergoes a phase transition from a semimetal to an insulator by charge-density-wave formation. This expectation is motivated by the potentially large value of the effective "fine-structure constant" $\alpha = e^2/(4\pi\hbar v_F \varepsilon) \sim O(1)$ when the dielectric constant ε is of the same order as one would expect for suspended graphene with $\varepsilon = 1$.

The critical coupling for this semimetal-insulator transition has been estimated theoretically in a variety of ways, generally yielding values of $\alpha_c \sim 1$ when no additional screening effects on the Coulomb interactions between the electrons in the graphene π bands, e.g., from electrons in the σ band, are included. A value of $\alpha_c = 0.92$ was obtained in Ref. 22 from a bifurcation analysis of a simplified gap equation in which radiative corrections to the Fermi velocity were neglected. A particular form for a momentum-dependent Fermi velocity renormalization based on a large-N expansion was used in Ref. 27 to obtain $\alpha_c = 1.13$. A renormalization group (RG) calculation at two-loop order yielded $\alpha_c = 0.833$.[28] Lattice studies have reported from Monte Carlo simulations on both standard square[29] and physical hexagonal[30] lattices $\alpha_c = 1.08 \pm 0.05$ and 0.9 ± 0.2, respectively. All these values are well below the bare coupling constant of suspended graphene, $\alpha_0 = 2.19$ with $\varepsilon = 1$, and thus in apparent contradiction with the experimental observation that suspended graphene remains in the semimetal phase.[11,25]

One possible explanation of this discrepancy might be the additional screening of the Coulomb interaction due to the other electrons, notably those in the σ band. In a constrained random phase approximation, these were indeed found to reduce the onsite repulsion and the first three nearest-neighbor Coulomb interaction parameters by successively decreasing factors between 1.8 and 1.3.[31] In a recent Monte Carlo simulation,[32] these parameters were used together with a corresponding screening of the long-range Coulomb tails to effectively reduce the interaction strength by an amount

which was found to be sufficient to place suspended graphene in the semimetal phase. While the additional screening of the short-range part of the π-band electrons' Coulomb interactions should certainly be included in a more quantitative calculation, here we focus on qualitative effects of their long-range Coulomb tails which one would in fact not expect to be screened by the other, localized electron states. A realistic description will probably have to include the right balance of all effects, the correct amount of onsite repulsion, favoring an antiferromagnetic Mott state,[33] the screening of the nearest-neighbor and short-range interactions which would otherwise lead to charge-density-wave formation,[34,35] as well as unscreened long-range Coulomb tails which might enhance the latter. Even if the strengths of these competing effects are all too weak for an insulating ground state in suspended graphene, it will be interesting to find out whether it is at least close to a possible transition into any one of the insulating phases (gapped spin-liquid[36] and topological insulator phases[37] have also been discussed).

Whatever the final answer will be, the experimentally observed reshaping of the Dirac cones in suspended graphene[11,25] does indicate that the Coulomb interactions induce a charge-carrier-density–dependent renormalization of the Fermi velocity. This renormalization peaks at half-filling where it leads to an increase by about a factor of 3 in the Fermi velocity and thus a corresponding decrease in the renormalized effective coupling. A momentum dependence of the Fermi velocity of a similar kind was in fact already predicted in an early perturbative RG study,[38] long before the synthesis of graphene. There, it was even concluded that v_F should keep growing logarithmically until retardation effects become important enough to invalidate the instantaneous Coulomb approximation.

Lattice simulations certainly have the potential to provide reliable results also for strongly coupled condensed matter systems, if the bare interactions are chosen correctly to describe the physical system. Even if the microscopic theory is completely specified as in QCD, however, continuum (at least in the time discretization), infinite volume, and chiral extrapolations are often difficult and expensive. This is very much so for the simulations of the electronic properties of graphene also. Moreover, a chemical potential for charge-carrier densities away from half-filling, e.g., to study the effects of interactions on the electronic Lifshitz transition of the free tight-binding model,[14] introduces a fermion sign problem here as well. Nonperturbative continuum approaches such as the functional renormalization group or Dyson-Schwinger equations therefore provide valuable alternatives. Especially when the necessary truncations are tested against lattice simulations in finite systems, without massless fermions and sign problem, the corresponding limits as well as finite density effects are relatively straightforwardly addressed with these functional continuum methods. In this paper, we employ the Dyson-Schwinger approach, which has been successfully applied to both QCD and three-dimensional QED (see, for example, Refs. 39–46 and references therein). In particular, we study the running of the Fermi velocity from Coulomb interactions in the Dirac-cone approximation, and its influence on the critical coupling for the semimetal-insulator transition by charge-density-wave formation in the effective low-energy model. To this end, we extend the study of Ref. 22 by first calculating the running Fermi velocity in various approximations for the particle-hole polarization. The results are qualitatively in line with the observed reshaping of the Dirac cones. In order to then determine the corresponding values for the critical coupling, we numerically solve the coupled system of Dyson-Schwinger equations for the fermion propagator with and without running Fermi velocity for comparison. We generally observe that the resulting critical coupling substantially increases when the strong renormalization effects in the Fermi velocity are included, thus favoring the persistence of suspended graphene in the semimetal phase. This general trend has also been observed in our preliminary analysis[47] in which we employed a GW approximation, in addition, in order to compute the Fermi velocity renormalization analytically.

The paper is organized as follows: In the next section, we briefly review the continuum model of graphene which is a variant of QED_3 with instantaneous bare Coulomb interactions. In Sec. III, we discuss the Dyson-Schwinger equation (DSE) for the fermion propagator in this model and present our solutions for the different particle-hole polarizations. Thereby, we first describe the results from a bifurcation analysis to find the critical point in Sec. III A. Our iterative numerical solutions of the full system of coupled integral equations are then presented in Sec. III B. Thereby we verify the bifurcation analysis and obtain complete results for the fermion mass and Fermi velocity renormalization functions in both phases. We compare our results for α_c to the literature on the DSE approach and assess the validity of the various approximation schemes. Moreover, we discuss the behavior of the pseudocritical coupling with explicit symmetry breaking by a staggered chemical potential, and the dependence of the critical coupling in the chiral limit on the number of fermion flavors providing evidence of Miranski scaling. Our summary and outlook are provided in Sec. IV.

II. DETAILS OF THE MODEL

In this paper, we study a low-energy continuum model for the long-range Coulomb interactions between the charge carriers in monolayer graphene, as previously considered in Refs. 22 and 48–51. In this model, the quasiparticle excitations at energies well below the van Hove singularity, around the two Dirac points within the first Brillouin zone of the honeycomb lattice, are described by massless Dirac fermions in two spatial dimensions. The honeycomb lattice is built from two independent triangular sublattices, corresponding to a triangular Bravais lattice with a two-component basis. Consequently, four-component Dirac spinors are introduced for the quasiparticle excitations on both sublattices A and B, each with momenta close to either of the two inequivalent Dirac points K (plus sign) and K' (minus sign), $\psi^T = (\psi^B_{+s}, \psi^A_{+s}, \psi^A_{-s}, \psi^B_{-s})$. The true spin of the electrons formally appears as an additional flavor quantum number $s = 1, \ldots, N_f$ with $N_f = 2$ for monolayer graphene. The graphene model is then specified by the action (in natural units with $\hbar = c = 1$)

$$\mathcal{S} = \int dt\, d^2r\ \bar{\psi}(t,\vec{r})[\mathrm{i}\gamma^0\partial_t - \mathrm{i}v_F\gamma^i\partial_i]\psi(t,\vec{r}) + \mathcal{S}_{\mathrm{int}}, \tag{2.1}$$

where $v_F \approx \frac{1}{300}$ is the Fermi velocity (we will return to its definition in the next section), ψ and $\bar{\psi} = \psi^\dagger \gamma^0$ denote the pseudo-spin-$\frac{1}{2}$ fermion field and its Dirac adjoint. The spatial index is $i = 1,2$, and the three four-dimensional γ matrices reducibly represent the Clifford algebra $\{\gamma^\mu,\gamma^\nu\} = 2g^{\mu\nu}$ in $2+1$ dimensions. In absence of magnetic fields and with $v_F \ll 1$, the electromagnetic interactions reduce to the purely electric coupling with the zero component of the photon field, initially in $3+1$ dimensions [with $\vec{x} = (\vec{r},z)$] and Feynman gauge,

$$\mathcal{S}_{\rm int} = \int dt\, d^3x \Big[-\rho(t,\vec{x})A^0(t,\vec{x}) + \frac{1}{2}[\vec{\nabla}A^0(t,\vec{x})]^2 - \frac{1}{2}(\partial_0 A^0(t,\vec{x}))^2 \Big], \quad \text{with}$$
$$\rho(t,\vec{x}) = e\bar{\psi}(t,\vec{r})\gamma^0\psi(t,\vec{r})\delta(z). \tag{2.2}$$

Magnetic interactions with the spatial vector components of the photon field could be introduced via Peierls substitution but are $O(v_F)$ suppressed and hence neglected. Consequently, the bare photon propagator in the $z = 0$ plane is simply given by

$$D^{00}_{\rm tl}(t,\vec{r},z=0) = \int \frac{d\omega}{2\pi}\frac{d^2k}{(2\pi)^2}\frac{dk_z}{2\pi}\frac{-{\rm i}}{\omega^2 - \vec{k}^2 - k_z^2 + {\rm i}\epsilon} \times e^{-{\rm i}\omega t}e^{{\rm i}\vec{k}\vec{r}}. \tag{2.3}$$

Integration over the perpendicular k_z-momentum modes of the Coulomb photon in the instantaneous approximation[38] then yields the dimensionally reduced, so-called "brane action," for the quasiparticles[50] with Coulomb interactions as usually employed in condensed matter systems,

$$\mathcal{S} = \int dt\, d^2r\, \bar{\psi}(t,\vec{r})[{\rm i}\gamma^0\partial_t - {\rm i}v_F\gamma^i\partial_i]\psi(t,\vec{r}) - \frac{e^2}{8\pi\varepsilon}\int dt\, d^2r\, d^2r'\, \bar{\psi}(t,\vec{r})\gamma^0\psi(t,\vec{r}) \times \frac{1}{|\vec{r}-\vec{r}'|}\bar{\psi}(t,\vec{r}')\gamma^0\psi(t,\vec{r}'). \tag{2.4}$$

Here, we have also introduced a dielectric constant $\varepsilon = (1+\kappa)/2$ to model the screening of the Coulomb interactions on top of a substrate, typically with $\kappa \approx 4$ for SiO_2 or $\kappa \approx 10$ for SiC, instead of $\varepsilon = 1$ for suspended graphene [neglecting the additional short-range screening from the localized electron states in graphene here, which would require a momentum dependent $\varepsilon(\vec{k})$ (Ref. 31)]. As discussed in the following, the bare Coulomb propagator is further modified due to the interactions by the particle-hole polarizability $\Pi(\omega,\vec{k})$, or Lindhard function of the electrons in the π bands.

The Feynman rules for the model are specified by the tree-level electron propagator and the fermion-photon vertex. These can be read off from the action as specified by Eqs. (2.1) and (2.2) to have the usual form with dimensionless charge despite the reduced dimensionality of the brane action

$$S^{-1}_{\rm tl}(p_0,\vec{p}) = -{\rm i}(\gamma^0 p_0 - v_F\gamma^i p_i), \tag{2.5}$$

$$\Gamma^0_{\rm tl}(k,p) = -{\rm i}e\gamma^0. \tag{2.6}$$

In addition to the tree-level quantities, we will also require the general decomposition for the fermion propagator $S(p)$. Because of the anisotropy introduced by the Fermi velocity, we need to treat temporal and spatial components separately:

$$S(p) = \frac{{\rm i}[Z(p)\gamma^0 p_0 - v_F A(p)\gamma^i p_i + \Delta(p)]}{Z^2(p)\,p_0^2 - v_F^2 A^2(p)\,\vec{p}^{\,2} - \Delta^2(p) + {\rm i}\epsilon}, \tag{2.7}$$

where $Z(p)$ is the wave-function renormalization, $A(p)$ is the Fermi velocity dressing function, and $\Delta(p)$ is the quasiparticle gap or mass function. These quantities can be obtained by solving numerically the Dyson-Schwinger equation for the fermion propagator. The determination of the critical point, along with the corrections introduced by the Fermi velocity renormalization, will be discussed in the next section.

III. DYSON-SCHWINGER EQUATIONS

Starting from the action in Eq. (2.4), the fermion Dyson-Schwinger (gap) equation follows with standard techniques:

$$S^{-1}(p_0,\vec{p}) = S^{-1}_{\rm tl}(p_0,\vec{p}) + {\rm i}e\int \frac{d^3k}{(2\pi)^3}\,\gamma^0 S(k_0,\vec{k})\Gamma^0(k,p) \times D_C(p_0-k_0,\vec{p}-\vec{k}), \tag{3.1}$$

where $\Gamma^0(k,p)$ is the fully dressed fermion-photon vertex depending on the incoming and outgoing fermion momenta. $D_C(q_0,\vec{q})$ is the dimensionally reduced, instantaneous Coulomb propagator with frequency-dependent Lindhard screening via the inclusion of the collective particle-hole polarizability. In the random phase approximation (RPA), with the one-loop expression for the polarization function $\Pi(q_0,\vec{q})$, it is given by[48]

$$D_C(q_0,\vec{q}) = \frac{\rm i}{2|\vec{q}| + \Pi(q_0,\vec{q})} \quad \text{with}$$
$$\Pi(q_0,\vec{q}) = \frac{e^2 N_f}{8\varepsilon}\frac{\vec{q}^{\,2}}{\sqrt{v_F^2\vec{q}^{\,2} - q_0^2}}. \tag{3.2}$$

Note, however, that by definition this one-loop expression for $\Pi(q_0,\vec{q})$ does not include radiative corrections to the Fermi velocity due to the renormalization function $A(p)$. As we will demonstrate explicitly below, strong Fermi velocity renormalization effects indeed tend to suppress the Lindhard screening, whose effect on the bare Coulomb interaction is hence overestimated by the one-loop polarizability $\Pi(q_0,\vec{q})$ in Eq. (3.2). In the static limit $q_0 \to 0$, the fully instantaneous RPA Coulomb propagator simply reduces to the bare one with constant Lindhard screening

$$\Pi(0,\vec{q}) = \frac{e^2 N_f}{8\varepsilon}\frac{|\vec{q}|}{v_F} = 2g|\vec{q}| \quad \text{and} \quad D_C(0,\vec{q}) = \frac{1}{1+g}\frac{\rm i}{2|\vec{q}|}, \tag{3.3}$$

where $g = \alpha_\varepsilon N_f \pi/4$ and $\alpha_\varepsilon = e^2/(4\pi v_F \varepsilon)$.

We now proceed with Dirac projection and Wick rotation to Euclidian space ($k_0 \to i\omega$). With the fully instantaneous Coulomb interaction, both the Fermi velocity and mass renormalization functions remain frequency independent, $A \equiv A(\vec{p})$ and $\Delta \equiv \Delta(\vec{p})$. One then furthermore has $Z = 1$ and, hence, as a consequence of the Ward-Takahashi identity, also

$\Gamma^0 = \Gamma^0_{\rm tl}$. As long as the frequency dependence in the Lindhard screening remains weak, one may therefore assume that, as a good first approximation, wave-function renormalization, vertex corrections, and the frequency dependencies in A and Δ can still be neglected. In this approximation, setting $p_0 = 0$ in the DSE (3.1), one obtains the following system of coupled integral equations for the fermion dressing functions $A(\vec{p})$ and $\Delta(\vec{p})$ (Ref. 22):

$$A(\vec{p}) = 1 + \alpha_\varepsilon v_F \int_{-\infty}^{\infty} \frac{d\omega}{2\pi} \int \frac{d^2\vec{k}}{(2\pi)^2} \frac{\vec{p}\,\vec{k}}{\vec{p}^{\,2}} \frac{A(\vec{k})}{\omega^2 + v_F^2 A^2(\vec{k})\vec{k}^2 + \Delta^2(\vec{k})} [-4\pi \mathrm{i}\, D_C(\mathrm{i}\omega, \vec{p} - \vec{k})], \tag{3.4}$$

$$\Delta(\vec{p}) = \alpha_\varepsilon v_F \int_{-\infty}^{\infty} \frac{d\omega}{2\pi} \int \frac{d^2\vec{k}}{(2\pi)^2} \frac{\Delta(\vec{k})}{\omega^2 + v_F^2 A^2(\vec{k})\vec{k}^2 + \Delta^2(\vec{k})} [-4\pi \mathrm{i}\, D_C(\mathrm{i}\omega, \vec{p} - \vec{k})]. \tag{3.5}$$

The temporal integration with the RPA Coulomb propagator in Eq. (3.2),

$$I(\vec{p},\vec{k}) = \int_{-\infty}^{\infty} \frac{d\omega}{2\pi} \frac{-4\pi \mathrm{i}\, D_C(\mathrm{i}\omega, \vec{p} - \vec{k})}{\omega^2 + v_F^2 \vec{k}^2 A(\vec{k})^2 + \Delta(\vec{k})^2}, \tag{3.6}$$

has already been performed in Ref. 22. It is given by [note the explicit inclusion of the bare Fermi velocity v_f here, as compared to Ref. 22 in which $v_F = 1$ was used in both the fermion DSE (3.1) and the RPA Coulomb propagator (3.2)]

$$I(\vec{p},\vec{k}) = \frac{J(z,g)}{|\vec{p} - \vec{k}| \sqrt{v_F^2 \vec{k}^2 A^2 + \Delta^2}}, \quad \text{with} \quad z = \frac{\sqrt{\vec{k}^2 A^2 + \Delta^2 / v_F^2}}{|\vec{p} - \vec{k}|}, \tag{3.7}$$

and $J(z,g)$ as a piecewise-defined function

$$J(z,g) = \frac{(z^2 - 1)[\pi - g c(z)] + z g^2 c(g)}{z^2 + g^2 - 1}, \quad \text{with} \quad c(x) = \begin{cases} 2\,\mathrm{arccosh}(x)/\sqrt{x^2 - 1}, & x > 1 \\ 2\arccos(x)/\sqrt{1 - x^2}, & x < 1 \\ 2, & x = 1. \end{cases} \tag{3.8}$$

With bare ($\Pi = 0$) and fully instantaneous RPA [$\Pi = 2g|\vec{q}|$, cf., Eq. (3.3)] Coulomb interactions, one has

$$J(z,g) = \pi \quad \text{and} \quad J(z,g) = \frac{\pi}{1 + g}, \tag{3.9}$$

respectively. In both these cases, J is independent of the fermion dressing functions A and Δ. We will also use these two simple special cases in our analysis of the critical coupling for comparison in the following.

A. Critical point analysis

For studying the dynamics at the critical point, an appropriate mathematical tool is bifurcation theory.[52] In this framework, the nonlinear equations simplify such that the critical coupling α_c, where the nontrivial solution of the gap equation bifurcates away from the trivial one, can be evaluated. Explicitly, applying bifurcation theory amounts to expanding Eqs. (3.4) and (3.5) to leading order Δ. This means using $\Delta = 0$ in (3.4), i.e., to solve for A in the symmetric phase, and expanding the right-hand side of Eq. (3.5) to linear order in Δ. In the Dirac-cone approximation, we furthermore have rotational invariance, and we can hence write $A(\vec{p}) = A(p)$ and $\Delta(\vec{p}) = \Delta(p)$ from now on with the notation $p \equiv |\vec{p}|$ for the magnitude of the spatial quasiparticle momentum

$$A(p) = 1 + \frac{\alpha_\varepsilon}{2\pi^2} \frac{1}{p} \int_0^\Lambda dk\, k \int_0^\pi d\theta \frac{\cos\theta}{\sqrt{p^2 + k^2 - 2\,p\,k\,\cos\theta}} \times J(z_0,g), \tag{3.10}$$

$$\Delta(p) = \frac{\alpha_\varepsilon}{2\pi^2} \int_0^\Lambda dk \int_0^\pi d\theta \frac{1}{\sqrt{p^2 + k^2 - 2\,p\,k\,\cos\theta}} \times \frac{\Delta(k)}{A(k)} J(z_0,g). \tag{3.11}$$

Here, $J(z,g)$ is either given by Eq. (3.8) and now $z_0 = A(k)\,k/|\vec{p} - \vec{k}|$ for $\Delta = 0$, or simply with either of the two constant values in (3.9). In the symmetric phase up to and, at a continuous transition, including the critical point, the integral equation (3.10) for the Fermi velocity renormalization A can be solved independently. In the broken phase, this solution for $\Delta = 0$ will of course not be the thermodynamically favored one. For the bifurcation analysis it can, however, be inserted into Eq. (3.11), in order to evaluate the critical coupling numerically, by a variant of the so-called power method.[53]

We emphasize that we solve all angular integrals numerically, thus avoiding further angle approximations as used in many previous studies. Moreover, it is also worth mentioning that the linearized equations can be solved much faster than the full nonlinear ones because the critical slowing down observed for the latter ones as the critical coupling is approached does not occur in the linearized problem. In order to obtain sufficiently precise values for α_c, it is crucial to use an extremely low-momentum cutoff in the infrared. It has been shown in Refs. 54 and 55 that the critical number of fermion flavors in ordinary QED$_3$, for example, is very sensitive to finite volume effects and thus to the infrared cutoff of the theory.

TABLE I. Critical couplings in various approximations for the particle-hole polarizability Π with and without Fermi velocity renormalization $A(p)$.

α_c	$\Pi = 0$	$\Pi_{\text{inst.}}$	$\Pi_{\text{one-loop}}$
$A = 1$	0.457(3)	1.63(2)	0.81(1)
$A(p)$	1.21(1)	∞	7.65(5)

We observe a similar phenomenon in the graphene version of QED_3 considered here. In our numerical integrals, we need infrared cutoffs of the order of $p^2 \sim 10^{-10}\Lambda^2$ to obtain reliable values of α_c, with controllable systematics. In the $\Pi = 0$ case, we could furthermore compare our numerical calculation with an analytical result of $\alpha_c^{\Pi=0} = 8\pi^2/\Gamma^4(1/4) \approx 0.457$ by Gusynin and collaborators[56,57] which then yielded very good agreement, with errors below the 1% level (see following).

The resulting values of the critical couplings for chiral symmetry breaking with $N_f = 2$ for monolayer graphene in the various approximations are summarized in Table I: the error bars reflect our numerical error estimated from comparison with our results from solving the set of nonlinear equations detailed in the following. Compared are the results from the three different approximations for the particle-hole polarization. For each of them we furthermore compare the solutions with self-consistent $A(p)$ and without Fermi velocity renormalization, i.e., $A = 1$. The difference between the upper and the lower rows in the table thus serves as a measure of the importance of including the nontrivial Fermi velocity renormalization function $A(p)$. Clearly, the effects are huge. Whereas for $\Pi = 0$ the critical coupling increases by a factor of about 2.5, there is no finite solution in the fully instantaneous approximation at all when $A(p)$ is dynamically included. This can be verified analytically because the instantaneous and bare Coulomb couplings α_0 and $\alpha_{\text{inst.}}$ from Eqs. (3.9) are simply related by

$$\alpha_{\text{inst.}}(\alpha_0) = \frac{2\alpha_0}{2 - \pi\alpha_0}. \tag{3.12}$$

Hence, $\alpha_{\text{inst.}}(0.457) = 1.62$, but $\alpha_{\text{inst.}}$ diverges at $\alpha_0 = 2/\pi \approx 0.64$ and there is no positive value for $\alpha_{\text{inst.}}$ above that, in particular at $\alpha_0 = 1.21$ with Fermi velocity renormalization. This is in agreement with our numerical analysis which fails to find a bifurcation point in this case. With the full RPA Coulomb interaction in (3.2) we obtain $\alpha_c \approx 0.81$ for $A = 1$ as compared to $\alpha_c \approx 0.92$ obtained in Ref. 22 from an analogous computation but with an additional angle approximation. Again, this value dramatically increases to $\alpha_c \approx 7.65$ when the self-consistent Fermi velocity renormalization $A(p)$ is included. The general trends can be understood as follows: static Lindhard screening increases the critical coupling too much because it clearly overestimates the screening effects by the particle-hole polarizability. These effects are somewhat reduced by including the frequency dependence in the Lindhard screening with the full RPA polarization. The strong Fermi velocity renormalization observed in all cases effectively weakens the Coulomb interaction and thus increases the critical coupling again. At the same time, however, one would expect that large deviations of $A(p)$ from $A = 1$ would effectively reduce the particle-hole polarizability again in a fully self-consistent solution of the fermion DSE together with that for the particle-hole polarization function Π, which would clearly be an important effect beyond RPA. In such a fully dynamic computation, one might expect two competing effects: A very large Fermi velocity renormalization would on one hand effectively switch off the Lindhard screening and hence tend to restore the bare Coulomb interactions. This, on the other hand, would in turn reduce the Fermi velocity renormalization to some degree again, not entirely though because it is still rather strong in our $\Pi = 0$ computation. Therefore, one might expect that the fully dynamical result should be somewhere between $\alpha_c \approx 1.21$ for $\Pi = 0$ and $\alpha_c \approx 7.65$ with the largely overestimated Lindhard screening in the RPA Coulomb interaction (3.2), when strong Fermi velocity renormalization effects occur.

In all approximations, we do observe a significant increase of $A(p)$ in the vicinity of the corresponding critical α_c such that $A(p)$ is significantly larger than one in the relevant momentum regime (see following). If plugged into the particle-hole polarization function, such large values of A would drastically suppress the polarization effects in the low-momentum region. As a result, the simple approximation $\Pi = 0$ might even be closer to the correct answer than the one-loop expression in Eq. (3.2). The final answer will have to await a fully dynamical and self-consistent simultaneous solution to both, the fermion DSE and the particle-hole polarization function (i.e., the Coulomb photon DSE).

The various results from Monte Carlo simulations within lattice gauge theory mentioned in the Introduction are all somewhat below our lower bound. Especially those by Drut and Lähde who obtained $\alpha_c = 1.08 \pm 0.05$ (Ref. 29) should be comparable to our results because they essentially use a discretized version of the same Dirac-cone approximation as the effective description for the low-energy electronic excitations of graphene, however, with full QED interactions. Quite obviously, retardation effects might become important with strong Fermi velocity renormalization.[38] These are beyond the instantaneous Coulomb interactions with frequency-dependent but nonrelativistic screening used here. For a more precise comparison between Dyson-Schwinger and lattice results, we should first include the photon polarization dynamically and self-consistently, however. Finite volume and finite mass effects could then be analyzed in more detail also in the DSE approach in order to be used for infinite volume and chiral extrapolations. (For a corresponding comparison in "ordinary" QED_3, see e.g. Refs. 54 and 55.)

B. Nonlinear equations

Having performed the bifurcation analysis which is appropriate precisely at the critical coupling, we now return to the original system of coupled (nonlinear) integral equations for the fermion propagator [Eqs. (3.4) and (3.5)]. To illustrate the potential effects of a large-A function, here we focus on the frequency-dependent RPA Coulomb interaction with the one-loop photon polarization function of Eq. (3.2). Explicitly, the equations then read as [with z now as given in (3.7), and

$g = \alpha_\varepsilon N_f \pi/4$ as before]

$$A(p) = 1 + \frac{\alpha_\varepsilon}{2\pi^2}\frac{1}{p}\int_0^\Lambda dk\, k \int_0^\pi d\theta \frac{\cos\theta}{\sqrt{p^2+k^2-2\,p\,k\,\cos\theta}} \times \frac{A(k)}{\sqrt{A^2(k)+\frac{\Delta^2(k)}{k^2 v_F^2}}} J(z,g), \tag{3.13}$$

$$\Delta(p) = m + \frac{\alpha_\varepsilon}{2\pi^2}\int_0^\Lambda dk \int_0^\pi d\theta \frac{1}{\sqrt{p^2+k^2-2\,p\,k\,\cos\theta}} \times \frac{\Delta(k)}{\sqrt{A^2(k)+\frac{\Delta^2(k)}{k^2 v_F^2}}} J(z,g), \tag{3.14}$$

where we have also included a small bare mass m via the tree-level propagator in the gap equation which acts as an external field for explicitly breaking the extended $U(2N_f)$ flavor symmetry of the low-energy theory down to $U(N_f) \times U(N_f)$ as discussed below.

In the nonlinear case, the critical coupling is obtained from evaluating the numerically determined mass function at zero momentum, in the chiral limit $m = 0$, which serves as an order parameter for chiral symmetry breaking together with an extrapolation towards the critical point using appropriate fit functions. Our numerical results together with the fits are shown in the left diagram of Fig. 1. Numerically, we seem to find an exponential decrease of the order parameter close to the critical coupling indicating Miransky scaling similar to the case of ordinary QED$_3$.[43,58,59] Indeed, a corresponding fit of the Miransky-type form

$$\Delta(0)/\Lambda = a_0 \exp\left(\frac{a_1}{\sqrt{\frac{1}{\alpha_c}-\frac{1}{\alpha}}}\right) \tag{3.15}$$

delivers excellent results with the parameters $a_0 = 6.4 \times 10^{-4}$, $a_1 = -0.138$, and a critical coupling of $\alpha_c = 7.68$. However, we also note that the fit form

$$\Delta(0)/\Lambda = \frac{|\alpha-\alpha_c|}{\left[\ln\left(\frac{a}{\alpha-\alpha_c}\right)\right]^3} \tag{3.16}$$

extracted from analytical results using an angular approximation[56] works equally well with the parameter $a = 345\,061$ resulting in $\alpha_c = 7.70$. The two values for the critical coupling obtained in this way are within the range $\alpha_c \approx 7.65(5)$ obtained from the bifurcation analysis in the last section.

To demonstrate the effects of the dynamical mass generation, we show in the right panel of Fig. 1 our numerical results for the Fermi velocity renormalization function at the couplings $\alpha = 6$ and 7 as well as $\alpha = 7.8$ and 9, below and above the critical coupling α_c. We notice that in the symmetric phase the self-consistent numerical solution for $A(p)$ contains a logarithmic divergence at $p^2 \to 0$ as in the GW approximation.[47] The slope of this logarithmic increase grows with α until the logarithmic infrared divergence gets suppressed due to the dynamical generation of a mass gap when the broken phase is reached such that $A(p)$ approaches a finite value for $\alpha > \alpha_c$ in the infrared. While a logarithmic behavior with further increasing slope persists for a certain range of intermediate momenta also in the broken phase above α_c, the saturation value in the infrared decreases with α from there on, and the momentum scale for this saturation hence increases. From an experimental point of view, the function A plays a very important role, as the Fermi velocity enters the mass function, and many other graphene observables. In fact, recent measurements[25] provide evidence that the spectrum of suspended graphene is indeed approximately logarithmic instead of linear near charge neutrality. This logarithmic increase would eventually invalidate the instantaneous Coulomb approximation for the electron interactions in graphene as pointed out in Ref. 38 already. Phenomenologically, on the other hand, the smallest momenta reached in experiments are limited by the finite size of realistic graphene sheets. For

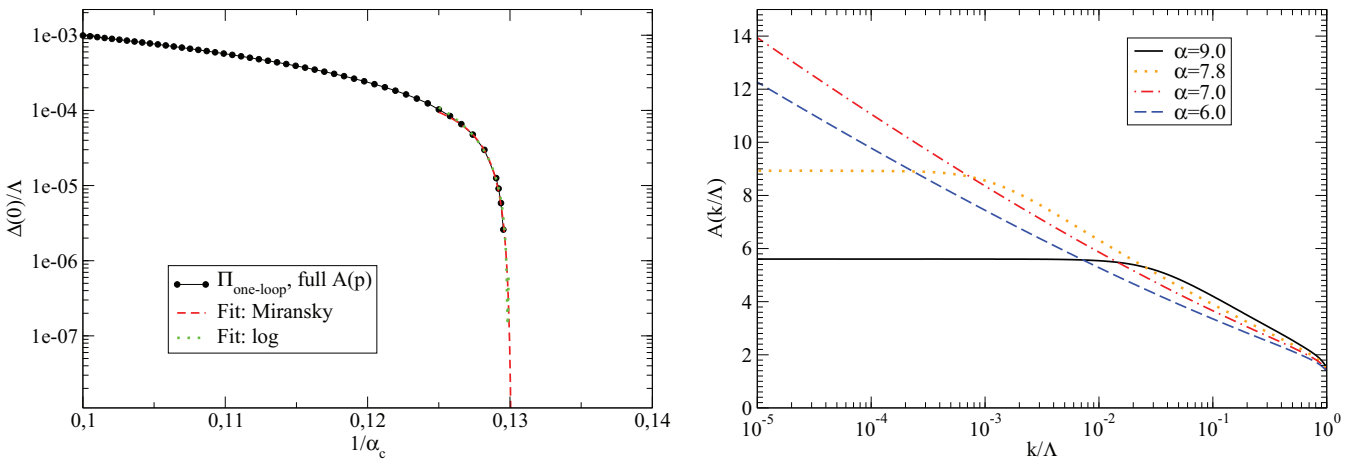

FIG. 1. (Color online) Left: fermion mass function at zero momentum over the inverse coupling $1/\alpha$ together with two fits for values of the coupling close to the critical one (see text for details). Right: momentum dependence of the Fermi velocity dressing function, exemplified for the couplings $\alpha = 6.0, 7.0, 7.8$ and $\alpha = 9.0$, below and above the corresponding critical coupling $\alpha_c \approx 7.65(5)$, respectively. Note the logarithmic infrared divergence in the results for $\alpha = 6.0, 7.0$, whereas for $\alpha = 7.8, 9.0$ this infrared divergence is screened by the dynamically generated mass. All results are for $N_f = 2$ here (see text for further details).

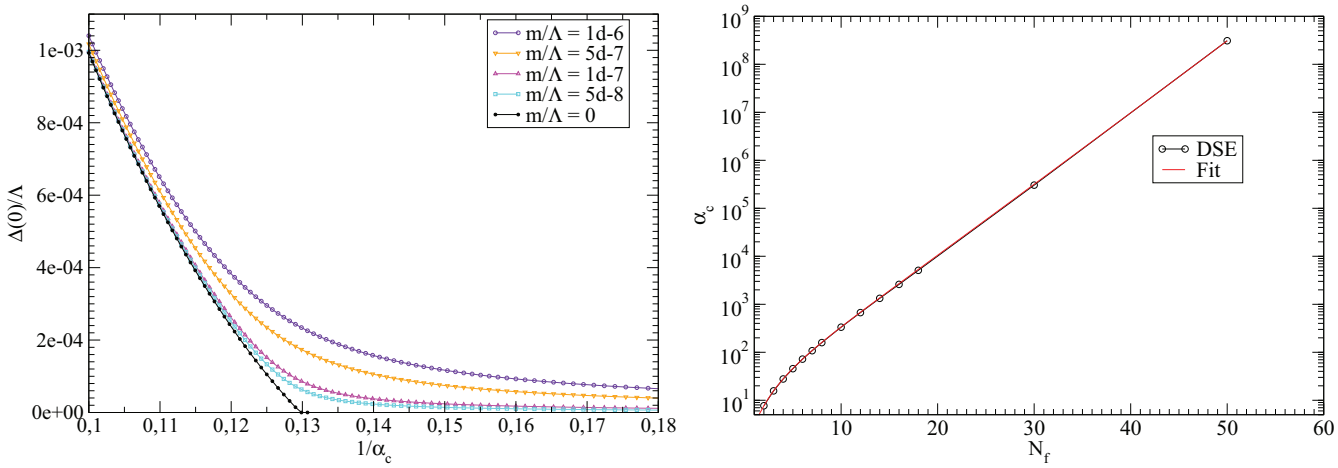

FIG. 2. (Color online) Left: mass dependence of the order parameter for $N_f = 2$. Right: large-N_f dependence of the critical coupling.

those, one observes an increase of the Fermi velocity by a factor (e.g., of the order of 3 in Ref. 25). With our present results for the semimetal phase, it would typically take sheets that are larger by several orders of magnitude to increase this logarithmic Fermi velocity renormalization factor from 3 to say 10. With the bare $v_F/c \approx \frac{1}{300}$ this would still justify the instantaneous approximation with $Z = 1$, as explained below Eq. (3.3), reasonably well.

In order to study explicit symmetry-breaking effects, we have also determined the zero-momentum limit of the mass function for a range of bare fermion masses m. The corresponding results are plotted as a family of functions over the inverse coupling in the left panel of Fig. 2. The general pattern is similar to the one seen in the lattice simulations.[29] The critical scaling is quite different, however. While infinite volume extrapolations of lattice results have provided evidence of a second-order phase transition with associated critical exponents, here we observe the typical Miransky scaling of QED_3 in the continuum approach as mentioned above and discussed in more detail in Ref. 22. Consequently, the magnetic scaling of the order parameter with the mass at the critical coupling is different from that in Ref. 29. Whether the infinite volume and chiral limit extrapolations are reliable in such a case is not clear to us.

The explicit symmetry breaking by $m \neq 0$ could be due to a staggered chemical potential with opposite signs on the two sublattices as induced by a sublattice-dependent substrate, for example. It would then be a seed for site-centered charge-density-wave formation and as such break parity. There are other Dirac mass terms which lead to the same general breaking pattern of the extended flavor symmetry $U(2N_f) \to U(N_f) \times U(N_f)$, but rather correspond to bond-ordered phases,[15] however. The main difference is whether the residual $U(N_f) \times U(N_f)$ mixes the two Dirac points or not.[23,60] This can not be distinguished on the level of the gap equation because it depends on the particular choice of the basis used for the reducible four-dimensional representation of the γ matrices which we did not have to specify in the derivation of Eq. (3.14). (Yet another realization of the same symmetry-breaking pattern is possible when the sign of the mass term is made spin dependent as it is actually done in lattice simulations to avoid the sign problem.[32] It then acts as an external field for antiferromagnetic order. To describe this, we would have to treat the $N_f = 2$ flavors separately here.)

Finally, let us shortly comment on the dependence of the critical coupling on the number of flavors N_f. The corresponding curve displayed in the right panel of Fig. 2 can be fitted with an expression of the form

$$f(N_f) = 12.7\, e^{\frac{N_f}{3}\sqrt{\frac{N_{fc}}{N_{fc}-N_f}}} - 14.4\, N_f^{0.25} \qquad (3.17)$$

from which we may read off a value for the critical number of (pseudo)fermion species of about $N_{fc} \sim 1200$ for which the critical coupling diverges. While this particular number is certainly not reliable for the reasons discussed above, the general finding of the very existence of a finite value for N_{fc} would confirm a conjecture of Son in Ref. 61. It remains to be seen, however, whether this result survives a self-consistent treatment of the particle-hole polarization function.

IV. SUMMARY AND OUTLOOK

In this study, we have determined critical couplings for the chiral phase transition from the fermion Dyson-Schwinger equation (DSE) with long-range Coulomb interactions in a low-energy model for monolayer graphene at half-filling. As compared to previous DSE studies of this model, we have dynamically included a nontrivial Fermi velocity dressing function in our self-consistent solutions for the fermion propagator. We have thereby compared the effects of static as well as fully frequency-dependent Lindhard screening with the bare Coulomb interaction. In all three cases, the self-consistent inclusion of the nontrivial Fermi velocity dressing function had dramatic effects, indicating that a substantial renormalization of the Fermi velocity should occur at strong coupling in agreement with experimental evidence from cyclotron-mass measurements in suspended graphene.[25] At the same time, such large Fermi velocity renormalizations also indicate that RPA Coulomb interactions with one-loop polarization function considerably overestimate the screening effects. Whether the screening is nevertheless strong enough for suspended graphene to remain in the semimetal phase remains to be

seen from a fully dynamical inclusion of the particle-hole polarization in a simultaneous solution of both the fermion and the Coulomb photon DSEs in the future.

Including the running Fermi velocity renormalization function, here we obtained $\alpha_c \approx 1.22$ for the critical coupling of the semimetal-insulator transition without screening as compared to $\alpha_c \approx 7.7$ with the fully frequency-dependent Lindhard screening in the RPA Coulomb interaction. We have argued that a self-consistent treatment of the particle-hole polarization should lead to a critical coupling between these two extremes with an expected tendency towards values closer to the lower bound. This leaves open the possibility that the critical coupling is larger than the bare coupling $\alpha_0 = 2.16$ for suspended graphene. Quite likely, however, additional screening from the electron states in the σ bands of graphene might have to be included in a more realistic calculation to achieve this.[31]

Although our study is indicative, a number of caveats remain. First of all, we need to include the particle-hole polarization effects dynamically and self-consistently to study their effect on α_c. When comparing with lattice results it will also be important to take finite volume effects into account. Finally, when comparing with experiment, other types of interactions such as four-fermion couplings might also be important and need to be included in the model. The first important steps in this direction have been discussed in Refs. 22 and 23.

Note added in proof. Recently, we have been made aware by G. Z. Liu of their related study in Ref. 62.

ACKNOWLEDGMENTS

We are grateful to V. P. Gusynin for pointing out numerical inaccuracies in a previous version of the manuscript and for sending us his private notes on analytical solutions of some of the equations. We would like to thank P. Buividovich, D. Mesterhazy, M. Ulybyshev, D. Smith, S. Strauss, and the late M. Polikarpov for helpful discussions. This work was supported by the Deutsche Forschungsgemeinschaft within SFB 634, by the Helmholtz Young Investigator Group Grant No. VH-NG-332, and by the European Commission, FP7-PEOPLE-2009-RG, Grant No. 249203.

[1] K. S. Novoselov, A. K. Geim, S. V. Morozov, D. Jiang, Y. Zhang, S. V. Dubonos, I. V. Grigorieva, and A. A. Firsov, Science **306**, 666 (2004).
[2] K. S. Novoselov, A. K. Geim, S. V. Morozov, D. Jiang, M. I. Katsnelson, I. V. Grigorieva, S. V. Dubonos, and A. A. Firsov, Nature (London) **438**, 197 (2005).
[3] V. P. Gusynin and S. G. Sharapov, Phys. Rev. Lett. **95**, 146801 (2005).
[4] Y. Zhang, Y.-W. Tan, H. L. Stormer, and P. Kim, Nature (London) **438**, 201 (2005).
[5] M. I. Katsnelson, K. S. Novoselov, and A. K. Geim, Nat. Phys. **2**, 620 (2006).
[6] V. V. Cheianov and V. I. Fal'Ko, Phys. Rev. B **74**, 041403 (2006).
[7] A. V. Rozhkov, G. Giavaras, Y. P. Bliokh, V. Freilikher, and F. Nori, Phys. Rep. **503**, 77 (2011).
[8] V. N. Kotov, B. Uchoa, and A. H. Castro Neto, Phys. Rev. B **78**, 035119 (2008).
[9] A. Castro Neto, F. Guinea, N. Peres, K. Novoselov, and A. Geim, Rev. Mod. Phys. **81**, 109 (2009).
[10] N. M. R. Peres, Rev. Mod. Phys. **82**, 2673 (2010).
[11] V. N. Kotov, B. Uchoa, V. M. Pereira, A. C. Neto, and F. Guinea, Rev. Mod. Phys. **84**, 1067 (2012).
[12] P. R. Wallace, Phys. Rev. **71**, 622 (1947).
[13] J. C. Slonczewski and P. R. Weiss, Phys. Rev. **109**, 272 (1958).
[14] B. Dietz, F. Iachello, M. Miski-Oglu, N. Pietralla, A. Richter, L. von Smekal, and J. Wambach, Phys. Rev. B **88**, 104101 (2013).
[15] C.-Y. Hou, C. Chamon, and C. Mudry, Phys. Rev. Lett. **98**, 186809 (2007).
[16] R. Jackiw and S.-Y. Pi, Phys. Rev. Lett. **98**, 266402 (2007).
[17] O. Oliveira, C. E. Cordeiro, A. Delfino, W. de Paula, and T. Frederico, Phys. Rev. B **83**, 155419 (2011).
[18] C. Popovici, O. Oliveira, W. de Paula, and T. Frederico, Phys. Rev. B **85**, 235424 (2012).
[19] A. Cortijo and M. A. Vozmediano, Nucl. Phys. B **763**, 293 (2007).
[20] J. K. Pachos and M. Stone, Int. J. Mod. Phys. B **21**, 5113 (2007).
[21] M. Vozmediano, M. Katsnelson, and F. Guinea, Phys. Rep. **496**, 109 (2010).
[22] O. V. Gamayun, E. V. Gorbar, and V. P. Gusynin, Phys. Rev. B **81**, 075429 (2010).
[23] D. Mesterhazy, J. Berges, and L. von Smekal, Phys. Rev. B **86**, 245431 (2012).
[24] L. Janssen and H. Gies, Phys. Rev. D **86**, 105007 (2012).
[25] D. C. Elias, R. V. Gorbachev, A. S. Mayorov, S. V. Morozov, A. A. Zhukov, P. Blake, L. A. Ponomarenko, I. V. Grigorieva, K. S. Novoselov, F. Guinea *et al.*, Nat. Phys. **8**, 172 (2012).
[26] A. Bostwick, J. L. McChesney, K. V. Emtsev, T. Seyller, K. Horn, S. D. Kevan, and E. Rotenberg, Phys. Rev. Lett. **103**, 056404 (2009).
[27] D. V. Khveshchenko, J. Phys.: Condens. Matter **21**, 075303 (2009).
[28] O. Vafek and M. J. Case, Phys. Rev. B **77**, 033410 (2008).
[29] J. E. Drut and T. A. Lähde, Phys. Rev. B **79**, 165425 (2009).
[30] P. Buividovich and M. Polikarpov, Phys. Rev. B **86**, 245117 (2012).
[31] T. O. Wehling, E. Şaşıoğlu, C. Friedrich, A. I. Lichtenstein, M. I. Katsnelson, and S. Blügel, Phys. Rev. Lett. **106**, 236805 (2011).
[32] M. Ulybyshev, P. Buividovich, M. Katsnelson, and M. Polikarpov, Phys. Rev. Lett. **111**, 056801 (2013).
[33] S. Sorella and E. Tosatti, Europhys. Lett. **19**, 699 (1992).
[34] I. F. Herbut, Phys. Rev. Lett. **97**, 146401 (2006).
[35] C. Honerkamp, Phys. Rev. Lett. **100**, 146404 (2008).
[36] Z. Y. Meng, T. C. Lang, S. Wessel, F. F. Assaad, and A. Muramatsu, Nature (London) **464**, 847 (2010).
[37] S. Raghu, X.-L. Qi, C. Honerkamp, and S.-C. Zhang, Phys. Rev. Lett. **100**, 156401 (2008).
[38] J. González, F. Guinea, and M. A. H. Vozmediano, Nucl. Phys. B **424**, 595 (1994).
[39] R. Alkofer and L. von Smekal, Phys. Rep. **353**, 281 (2001).
[40] P. Maris and C. D. Roberts, Int. J. Mod. Phys. E **12**, 297 (2003).
[41] C. S. Fischer, J. Phys. G **32**, R253 (2006).
[42] P. Maris, Phys. Rev. D **52**, 6087 (1995).
[43] C. S. Fischer, R. Alkofer, T. Dahm, and P. Maris, Phys. Rev. D **70**, 073007 (2004).

[44]J. A. Bonnet, C. S. Fischer, and R. Williams, Phys. Rev. B **84**, 024520 (2011).
[45]J. A. Bonnet and C. S. Fischer, Phys. Lett. B **718**, 532 (2012).
[46]C. Popovici, Mod. Phys. Lett. A **28**, 1330006 (2013).
[47]C. Popovici, C. Fischer, and L. von Smekal, PoS (**Confinement X**), 269 (2012).
[48]J. González, F. Guinea, and M. A. H. Vozmediano, Phys. Rev. B **59**, R2474 (1999).
[49]D. V. Khveshchenko, Phys. Rev. Lett. **87**, 246802 (2001).
[50]E. V. Gorbar, V. P. Gusynin, and V. A. Miransky, Phys. Rev. D **64**, 105028 (2001).
[51]E. V. Gorbar, V. P. Gusynin, V. A. Miransky, and I. A. Shovkovy, Phys. Rev. B **66**, 045108 (2002).
[52]D. Atkinson, J. C. R. Bloch, V. P. Gusynin, M. R. Pennington, and M. Reenders, Phys. Lett. B **329**, 117 (1994).
[53]J. Hoffman, *Numerical Methods for Engineers and Scientists* (McGraw-Hill, New York, 2001).
[54]V. P. Gusynin and M. Reenders, Phys. Rev. D **68**, 025017 (2003).
[55]T. Goecke, C. S. Fischer, and R. Williams, Phys. Rev. B **79**, 064513 (2009).
[56]V. Gusynin (private communication).
[57]O. V. Gamayun, E. V. Gorbar, and V. P. Gusynin, Phys. Rev. B **80**, 165429 (2009).
[58]V. A. Miransky and K. Yamawaki, Phys. Rev. D **55**, 5051 (1997).
[59]J. Braun, C. S. Fischer, and H. Gies, Phys. Rev. D **84**, 034045 (2011).
[60]V. P. Gusynin, S. G. Sharapov, and J. P. Carbotte, Int. J. Mod. Phys. B **21**, 4611 (2007).
[61]D. T. Son, Phys. Rev. B **75**, 235423 (2007).
[62]J.-R. Wang and G.-Z. Liu, New J. Phys. **14**, 043036 (2012).